Journal of Catalysis 383 (2020) 24–32

Contents lists available at ScienceDirect

Journal of Catalysis

journal homepage: www.elsevier.com/locate/jcat

Kinetics of aromatics hydrogenation on HBEA

Sukaran S. Arora, Aditya Bhan *

Department of Chemical Engineering and Materials Science, University of Minnesota, Minneapolis, MN 55455, USA

ARTICLE INFO

Article history:
Received 8 September 2019
Revised 16 December 2019
Accepted 27 December 2019

Keywords:
Aromatics hydrogenation
Brønsted acid zeolites
Kinetics
Ring reduction
Ring opening
HBEA
Methanol to hydrocarbons

ABSTRACT

Zeolite HBEA catalyzes hydrogenation of aromatic hydrocarbons—methyl-substituted benzenes (benzene and toluene), alkenyl-substituted benzenes (styrene), and polycyclics (naphthalene)—in presence of excess H_2 at high-temperatures (573–748 K) with rates that depend linearly on aromatic and H_2 pressures. The observed kinetic behavior can be rationalized based on a sequence of elementary steps where the first hydrogenation step of the adsorbed benzenic intermediate is rate-determining while subsequent hydrogenation and desorption steps are quasi-equilibrated and H^+ is the most abundant surface species. Styrene hydrogenation exhibits the highest rates among the aromatics considered and results exclusively in ethylbenzene synthesis; in contrast, benzene/toluene and naphthalene hydrogenation results in formation of their triply-hydrogenated five-membered ring and doubly-hydrogenated ring open analogs, respectively. Based on independent studies involving co-reaction of cyclohexene and 1-methyl-1-cyclopentene with H_2, we infer their facile interconversion and hydrogenation to methylcyclopentane implying that conversion of benzene to methylcyclopentane likely occurs via intervening formation of both five- and six-membered ring intermediates. Taken together, these studies demonstrate feasibility of aromatics hydrogenation and propensity of benzenic rings in these hydrocarbons to undergo ring reduction or ring opening during their activation with H_2 on Brønsted acid zeolites.

1. Introduction

The ability of Brønsted acid zeolites to activate H_2 for direct hydrogenation of olefins and monocyclic aromatics was initially demonstrated in the 1980s by Sano and co-workers [1–3], Gadalla et al. [4], and Kanai et al. [5]. Sano [6] implicated protons in HZSM-5 to be the active sites for hydrogenation of olefins by observing ~25%C selectivity of C_2–C_3 paraffins over a Fe/HZSM-5 sample (0.82 wt% Fe; Si/Al = 20) compared to ~1%C over a Fe/silicalite sample (2.2 wt% Fe) during CO hydrogenation (CO/H_2 ~1) at 673 K, 9.8 bar, 1000 h^{-1}. Along the same lines, Sano [6] demonstrated the role of protons in aromatics hydrogenation by showing that conversion levels of benzene (H/C = 1) during its co-reaction with excess H_2 (C_6H_6/H_2 = 3/97) at 846 K, 39.3 bar, 5000 h^{-1} over HZSM-5 samples with fixed Si/Al (~35) but with varying amounts of Fe (~0.009–0.7 wt%) did not vary significantly and H/C ratio of effluent products was ~1.4 over the sample with 0.009 wt% Fe loading compared to ~1.5 over samples with higher Fe contents. In their study, benzene hydrogenation resulted in the formation of methane, ethane, propane, toluene, and xylenes while direct hydrogenated analogs—cyclohexane and methylcyclopentane—were only observed at a lower temperature (573 K).

Several experimental [7–9] and theoretical reports [10,11] since have validated the ability of proton-form zeolites for catalyzing olefins hydrogenation and it has been proposed that in the kinetic regime where measured rates of alkane formation vary linearly with olefin and H_2 pressures, this reaction occurs via a set of elementary steps that are the microscopic reverse of steps involved in monomolecular dehydrogenation of paraffins [9]. Recent reports by Arora et al. [12,13], Nieskens et al. [14], and Zhao et al. [15] have demonstrated that the hydrogenation ability of acidic protons can be exploited to significantly improve catalyst lifetime (at least one order of magnitude enhancement in total turnover capacity) during methanol-to-hydrocarbons (MTH) conversion over Brønsted acid zeolites with H_2 cofeeds. The formation of formaldehyde in transfer dehydrogenation events involving methanol, and its involvement in electrophilic addition reactions with olefins and methyl-substituted benzenes facilitating the formation of polycyclics have been implicated as critical in catalyst deactivation during MTH (Scheme 1) [16–22]. The observed improvements in lifetime with H_2 cofeeds suggest that cofeeding H_2 intercepts formaldehyde-mediated alkylation pathways via preferential hydrogenation of unsaturated intermediates formed during polycyclics production. In support of this proposal, Arora et al.

* Corresponding author.
E-mail address: abhan@umn.edu (A. Bhan).

https://doi.org/10.1016/j.jcat.2019.12.039
0021-9517/

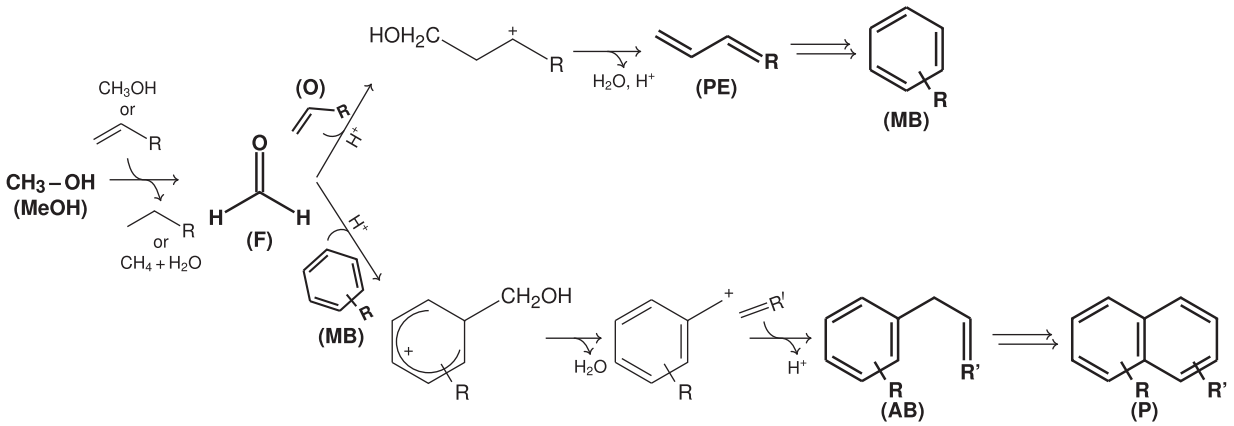

Scheme 1. Schematic illustrating formation of formaldehyde (F) from transfer dehydrogenation of methanol (MeOH), and its involvement in Prins reactions with olefins (O) and methyl-substituted benzenes (MB) resulting in synthesis of unsaturated intermediates—polyenes (PE) and alkenyl-substituted benzenes (AB)—that eventually transform to polycyclics (P) during MTH over Brønsted acid zeolites. Reaction scheme adapted from [19].

[13] carried out independent kinetic studies of ethene, propene, and 1,3-butadiene hydrogenation over various Brønsted acid zeolites (HSSZ-13, HSSZ-39, HFER, and HBEA) and noted that the measured hydrogenation rate constants of 1,3-butadiene were at least one order of magnitude (~7× to ~320×) higher than the corresponding values for ethene and propene over all zeolites considered. Further, Zhao et al. [15] showed that the composition of entrained hydrocarbons shifted from large polycyclics to light aromatics upon treatment of a deactivated HSAPO-34 sample with H_2. Although this demonstration, in addition to those reported by Sano and co-workers [2,3,6], evinces the ability of Brønsted acid zeolites to effect aromatics hydrogenation, no rates, mechanisms, or pathways of the involved reactions have been reported in the literature.

Herein, we present results from kinetic studies of benzene, toluene, styrene, and naphthalene hydrogenation over HBEA—a zeolite which exhibits a 3-dimensional system of mutually intersecting straight 12-membered ring channels with large pore openings (6.4 × 7.6 Å along [100] and 5.5 × 5.5 Å along [001]) that allow facile diffusion of aromatics [23]. The measured hydrogenation turnover rates (per H^+) are observed to depend linearly on reactant pressures in all cases and a sequence of elementary steps is presented to rationalize this behavior. Two distinct pathways are considered for hydrogenation of benzene to methylcyclopentane and a quantitative kinetic model is reported to ascribe the mechanism of ring reduction. The mechanistic origins of higher reactivity with H_2 exhibited by styrene and naphthalene compared to benzene/-toluene are also discussed and consequences of this reactivity trend are considered in context of MTH with H_2 cofeeds over Brønsted acid zeolites.

2. Materials and methods

2.1. Catalyst characterization

Zeolite BEA was sourced from Zeolyst (CP814E) in its ammonium-form and converted to proton-form by thermal treatment in flowing dry air (1.67 $cm^3\ s^{-1}$; Zero Grade, Matheson) at 823 K (0.0167 K s^{-1} ramp rate from RT) for 4 h. The framework type was confirmed as BEA by its powder X-ray diffraction pattern collected using a Bruker micro-diffractometer with Cu K_α (λ = 1.54 Å) as radiation source (Fig. S1a of SI). The t-plot micropore volume (0.16 $cm^3\ g^{-1}$) and Brunauer-Emmett-Teller (BET) surface area (530 $m^2\ g^{-1}$) of the sample were obtained from N_2 adsorption measurements collected at 77 K using an ASAP 2020 instrument (Micromeritics). Degassing was performed by evacuating the sample tube to ⩽ 10 μmHg at 363 K (0.083 K s^{-1} ramp rate from RT) followed by thermal treatment in vacuo at 723 K (0.083 K s^{-1} ramp rate from 363 K) for 4 h prior to N_2 adsorption; the observed isotherms are shown in Fig. S1b of SI. The average crystallite size of the sample was ascertained as ~0.25 μm from Scanning Electron Microscopy (SEM) images (Fig. S3 of SI). The bulk Si/Al atomic ratio of ~12.5 as determined from Scanning Electron Microscopy with Energy Dispersive X-ray Spectroscopy (SEM-EDS) measurements matched closely with the near-surface Si/Al ratio of 17.6 obtained from X-ray Photoelectron Spectroscopy (XPS) measurements indicating that Al atoms are uniformly distributed in the lattice. The SEM-EDS analysis also confirmed the absence of metallic impurities in the sample. The Brønsted acid site density was obtained from NH_3 temperature programmed desorption (0.33 mmol g^{-1}) and pyridine IR (0.26 mmol g^{-1}) measurements [13]. All rate constants presented herein are normalized by the site count obtained from NH_3 TPD measurement to be consistent with the procedure used in our recent report describing kinetics of aliphatics—ethene, propene, and 1,3-butadiene—hydrogenation on Brønsted acid zeolites [13].

2.2. Catalytic testing

All experiments were performed in a borosilicate glass-lined stainless steel reactor tube (6.35 mm outer diameter and 4 mm inner diameter; Scientific Glass Engineering). The proton-form sample was subject to pelletization, crushing, and sieving to retain 180–250 μm (60–80 mesh) aggregates which were physically mixed with aggregates of sand (Acros Organics; subjected prior to an overnight wash in 2 M HNO_3 solution followed by deionized water rinse until pH ~7, and a final thermal treatment in flowing dry air (1.67 $cm^3\ s^{-1}$; UHP Grade, Matheson) at 1273 K (0.083 K s^{-1} ramp rate from RT) for 16 h; $10 < wt_{diluent}/wt_{cat} < 15$) and packed in the middle of the reactor tube between quartz wool (Technical Glass Products) plugs. The tubular reactor was placed inside a resistively heated furnace (Model 3210, Applied Test Systems) regulated with an electronic controller (Series 96, Watlow). The reaction temperature was measured using a K-type thermocouple (TJ36-CAXL-020U-12, Omega) wrapped around the reactor periphery with tip placed near the axial-center. The free volume above and below the catalyst bed was filled by quartz rods (3 mm O.D.; Technical Glass Products) to prevent vertical displacement of the catalyst bed. Prior to catalytic measurements, the catalyst bed was pretreated in flowing dry air (1.67 $cm^3\ s^{-1}$) at 823 K (0.0167 K s^{-1} ramp rate from RT) for 4 h before being allowed to

cool to reaction temperature and being subject to a He (1.67 cm^3-s^{-1}; 99.997%, Matheson) purge at reaction temperature for ⩾2 h. All gas flows including H_2 (99.9999%, Matheson), He, and Ar (99.9995%, Matheson) were metered using mass flow controllers (Model 5850E, Brooks). Liquid reagents including benzene (⩾99.0%, ACS Reagent, Sigma–Aldrich), cyclohexene (⩾99.0%, Sigma–Aldrich), 1-methyl-1-cyclopentene (⩾98.0%, Sigma–Aldrich), toluene (⩾99.9%, HPLC Plus, Sigma–Aldrich), styrene (⩾99.0% with 4-*tert*-butylcatechol as stabilizer which was removed prior to use with an alumina-based inhibitor remover (product #306320, Sigma–Aldrich), ReagentPlus®, Sigma–Aldrich), ethylbenzene (99.8%, anhydrous, Sigma–Aldrich), and p-xylene (⩾99.0%, puriss. p.a., Sigma–Aldrich) were delivered using a syringe pump (Legato 100, KD Scientific), vaporized in heat traced lines (~358 K), and swept by the flowing gas stream. Since naphthalene (99%, Sigma–Aldrich) is a solid at room temperature, it was dissolved and fed as a mixture with benzene (naphthalene/benzene ~ 35). Cyclohexene, 1-methyl-1-cyclopentene, and styrene were also fed as a dilute mixture with toluene (R/toluene ~ 370–525) in order to obtain low inlet partial pressures (0.04–0.30 × 10^{-5} bar) which were necessary to eliminate any secondary reactions and to obtain high selectivity of primary products resulting from hydrogenation. Control experiments were performed with He cofeeds instead of H_2 in order to verify that observed products resulted from direct hydrogen transfer from H_2 and not from intermolecular hydrogen transfer between hydrocarbons. The total gas-phase pressure was measured using a pressure transducer (0–6890 kPag; PX32B1-1KGV, Omega) placed upstream of the reactor, and controlled using a back-pressure regulator (0–3440 kPag; 44–2300 series, Tescom) placed downstream of the reactor. The composition of effluent stream was characterized and quantified using a gas chromatograph (Model 7890A, Agilent) equipped with a dimethylpolysiloxane HP-1 column (50 m × 320 μm × 0.52 μm) connected in parallel to a flame ionization detector and a mass spectrometer (Model 5975C, Agilent) for detection of hydrocarbons, and a GS-GasPro column (60 m × 320 μm) connected to a thermal conductivity detector for detection of permanent gases (H_2 and Ar).

3. Results

3.1. Hydrogenation of methyl-substituted benzenes on HBEA

Benzene and toluene were chosen as representative unsubstituted and methyl-substituted benzenes in this study. Reactions of benzene and toluene with excess H_2 (H_2/R > 1500) at 673 K on HBEA under differential conditions (<0.1% conversion) resulted in the exclusive formation of methylcyclopentane in case of benzene, and a combination of dimethylcyclopentanes, ethylcyclopentane and methylcyclohexane in case of toluene as shown in Scheme 2 along with the measured selectivites. The measured hydrogenation rates in both cases were stable with time on stream demonstrating absence of catalyst deactivation (Fig. S2a-b of SI) and using the Weisz-Prater criterion [24] (Table S1 of SI), it was verified that measured rates were not corrupted by internal diffusion limitations. Further, measured hydrogenation rates in both cases varied insignificantly with space velocity of the aromatic (Fig. S4a-b of SI) evidencing no effects of secondary reactions or inhibition by products on measured rates. Fig. 1 shows that measured rates of benzene and toluene hydrogenation normalized by total Brønsted acid sites (H^+) in the catalyst bed depend linearly on partial pressure of the aromatic (p_R) and H_2 (p_{H_2}), and can be described quantitatively by the rate expression shown in Eq. (1).

$$\frac{r}{[H^+]} = k^R_{H_2} p_R p_{H_2}. \quad (1)$$

The term $k^R_{H_2}$ in Eq. (1) represents the effective second-order rate constant and can be enumerated as the slope of the linear fit to measured rates as a function of aromatic or H_2 pressure. The values thus obtained for benzene ($k^{C_6H_6}_{H_2}$) and toluene ($k^{C_7H_8}_{H_2}$) are (0.0012 ± 0.0002) and (0.0033 ± 0.0004), respectively, with corresponding units as mol $(mol\ H^+)^{-1}\ s^{-1}\ (bar\ R)^{-1}\ (bar\ H_2)^{-1}$. The temperature dependence of measured rate constants for both cases is shown in Fig. S5 of SI and can be described quantitatively by the Arrhenius equation shown in Eq. S1 of SI. This description combined with transition state theory also allows enumeration of apparent enthalpic and entropic barriers for their hydrogenation (see Section S4 of SI for details), and the corresponding values are tabulated in Table S2 of SI alongside their 95% confidence intervals. Benzene hydrogenation was also performed on a different HBEA sample (Zeolyst CP814C with bulk Si/Al ~19.8 as determined by SEM-EDS measurements which also confirmed absence of metallic impurities, and Brønsted acid site density of 0.16 mmol g^{-1} enumerated using NH_3 TPD measurements) as a control (see Section S5 of SI for details), and as shown in Fig. S7a, the observed hydrogenation rates are again observed to depend linearly on both benzene and H_2 pressures. The apparent enthalpic and entropic barriers for benzene hydrogenation calculated as (93 ± 12 kJ mol^{-1}) and (−207 ± 18 J $mol^{-1}\ K^{-1}$), respectively, from temperature dependence of measured rate constants shown in Fig. S7b are similar to

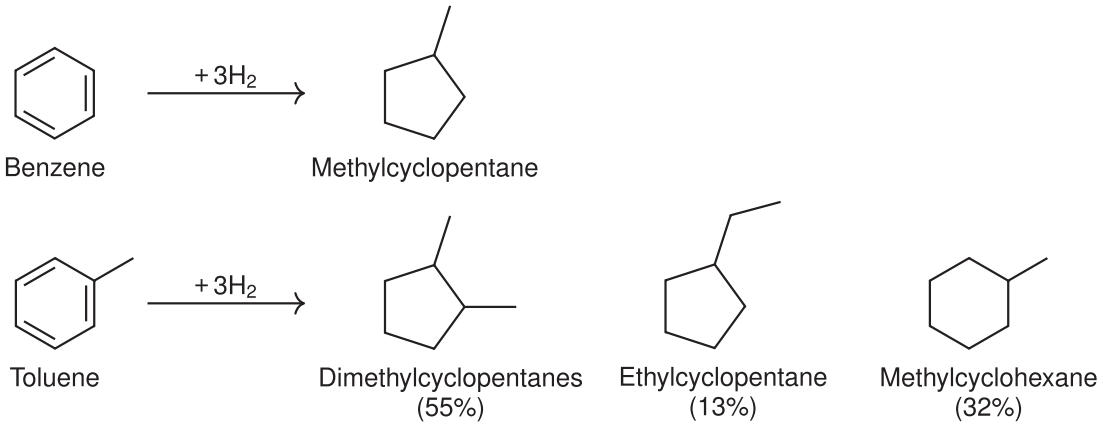

Scheme 2. Typical product distribution observed during benzene and toluene hydrogenation over HBEA at 673 K. The conversion level in case of toluene hydrogenation was ~0.06% during its feed at 0.0016 bar with 3.0 bar H_2 at 24.9 $mol_{C_7H8}\ (mol_{H^+} \cdot ks)^{-1}$ and 3.07 bar total pressure (including 0.068 bar Ar).

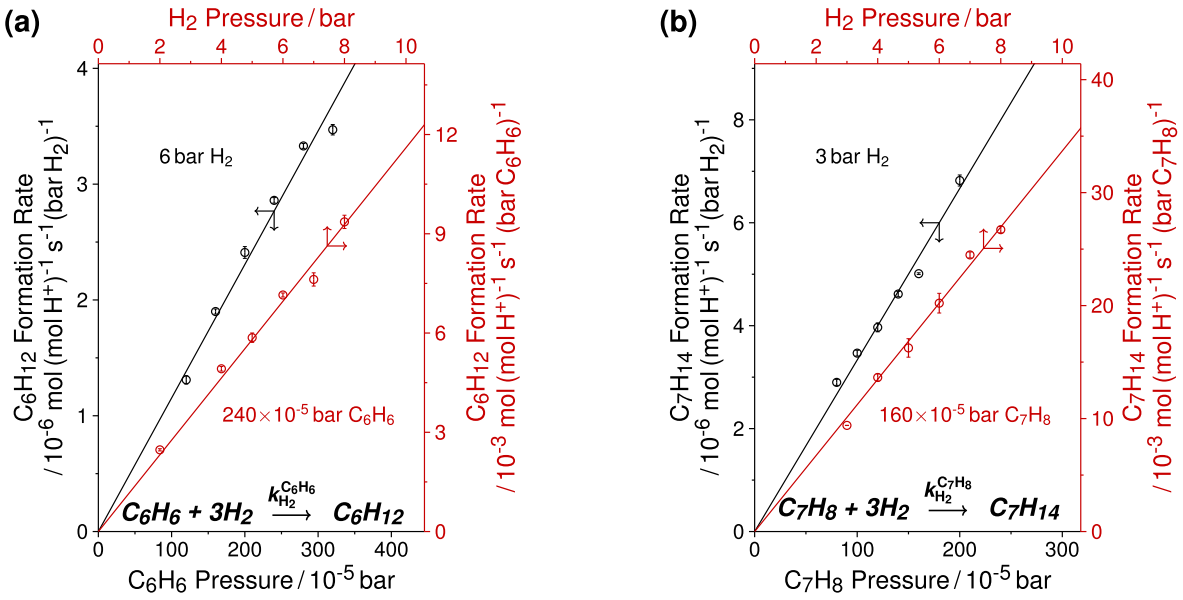

Fig. 1. Dependence of turnover rates (per H^+) of (a) benzene and (b) toluene hydrogenation on partial pressure of the aromatic (*bottom-left* axes) and H_2 (*top-right* axes) at 673 K and (a) 18.7–49.8 mol_{C_6H6} $(mol_{H^+}\cdot ks)^{-1}$; (b) 19.9–53.0 mol_{C_7H8} $(mol_{H^+}\cdot ks)^{-1}$ over HBEA. The solid lines represent a linear fit to experimental data and quantities listed along these lines indicate partial pressure of the aromatic or H_2 held constant while varying partial pressure of the other reagent. The vertical bars on each data point reflect standard-error associated with each measurement. The total gas-phase pressure of influent stream varied between 2.07–8.07 bar (including 0.068 bar Ar).

the values of (89 ± 11 kJ mol^{-1}) and (−196 ± 17 J mol^{-1} K^{-1}) obtained on the HBEA sample employed in this study.

The linear dependence of measured turnover rates (per H^+) of benzene and toluene hydrogenation on reactant pressures (Eq. (1)) can be rationalized by the set of elementary steps shown in Scheme 3 with the following assumptions: (i) the fourth step involving the first hydrogenation reaction between the proton-bound aromatic intermediate (RH^+) and intrazeolite H_2 species (H_2 (z)) is rate-determining; (ii) all subsequent hydrogenation reactions and steps involving adsorption/desorption of reactants and products are quasi-equilibrated; and (iii) H^+ are the most abundant surface species.

The selective formation of five-membered cycloalkanes during benzene and toluene hydrogenation (Scheme 5) is unlike what is observed over metallic catalysts that primarily form cyclohexane and methylcyclohexane, respectively [25,26]. This observation is, however, consistent with (i) higher thermodynamic stability of five-membered cycloalkanes compared to their six-membered ring analogs s (calculated ΔG_f^o (623 K) = −338.2 kJ mol^{-1} for methylcyclopentane compared to −329.9 kJ mol^{-1} for cyclohexane; detailed calculations presented in Section S6 of SI), and (ii) the ability of zeolitic protons to promote formation of carbenium ions that evolve through alkyl and hydride rearrangements towards thermodynamically stable forms [27–29]. The observed linear dependence of measured hydrogenation rates on reactant pressures and the inference that the first hydrogenation step is rate-determining implies it is kinetically infeasible to ascertain when ring reduction takes place since the intermediates generated will react rapidly to form the final products observed in the effluent. Scheme 4 illustrates two different pathways that can be involved in the conversion of benzene to methylcyclopentane. The top pathway involving intermediate formation of cyclohexadiene and cyclohexene is referred as the 'C6 pathway' while the bottom pathway involving intermediate formation of methylcyclopentadiene and methylcyclopentenes is referred as the 'C5 pathway'. The aforementioned conclusion regarding rapid disappearance of intermediates in case of benzene hydrogenation can then be mathematically stated as $k_2^{C6/C5}$ and $k_3^{C6/C5} \gg k_1^{C6/C5}$, where $k_2^{C6/C5}$ and $k_3^{C6/C5}$ represent hydrogenation rate constants of intermediates involved in the second and third hydrogenation steps, respectively, and $k_1^{C6/C5}$ represents the rate constant of the rate-determining first hydrogenation step of benzene. We carried out independent studies involving hydrogenation of cyclohexene and 1-methyl-1-cyclopentene over HBEA to enumerate k_3^{C6} and k_3^{C5} for comparison with $k_1^{C6/C5} (= k_{H_2}^{C_6H_6})$ reported earlier to verify the stated mathematical relation and ascertain if either pathway is preferred during benzene hydrogenation.

Co-feeding cyclohexene and 1-methyl-1-cyclopentene (both diluted with toluene) independently with excess H_2 (H_2/R > 33,000) resulted in methylcyclopentane formation; however, in both cases facile interconversion between cyclohexene and methylcyclopentenes was also observed independent of the cofeed identity among H_2 or He (Scheme 5 shows the effluent product distribution observed while independently feeding cyclohexene and 1-methyl-1-cyclopentene with H_2 under identical reaction conditions). In an effort to enumerate hydrogenation rate constants of cyclohexene and methylcyclopentene (k_3^{C6} and k_3^{C5}, respectively) while considering their disposition to interconvert, we considered an integral packed bed model with plug-flow hydrodynamics with the corresponding differential material balance equations shown in Eqs. (2)–(4).

$$\frac{d\dot{n}_i}{dw} = \sum_j r_{i,j}(k_j, p_j), \tag{2}$$

$$\left(\frac{\dot{V}}{RT}\right)\frac{d(p_i/p_o)}{d(w/w_o)} = \sum_j r_{i,j}(k_j, p_j/p_o) \times w_o, \tag{3}$$

$$\left(\frac{\dot{V}}{RT}\right)\frac{d(p_i/p_o)}{dy} = \sum_j r_{i,j}(k_j, p_j/p_o) \times w_o, \tag{4}$$

where $\dot{n}$ represents molar flow rate of species i measured at ambient conditions (295 K and 1 atm), w represents number of H^+ in the catalyst bed, $\sum_j r_{i,j}(k_j, p_j)$ represents net rate of formation of species i from j reactions as a function of k_j and p_j, k_j represents unknown rate constant of reaction j, p_i and p_j represent instantaneous partial

$R\,(g)$	$\underset{k_{-1}}{\overset{k_1}{\rightleftharpoons}}$	$R\,(z)$	K_1
$H_2\,(g)$	$\underset{k_{-2}}{\overset{k_2}{\rightleftharpoons}}$	$H_2\,(z)$	K_2
$R\,(z) + H^+$	$\underset{k_{-3}}{\overset{k_3}{\rightleftharpoons}}$	RH^+	K_3
$\mathbf{RH^+ + H_2\,(z)}$	$\boldsymbol{\xrightarrow{k_4}}$	$\mathbf{RH_3{}^+}$	$\boldsymbol{k_4}$
$RH_3{}^+ + H_2\,(z)$	$\underset{k_{-5}}{\overset{k_5}{\rightleftharpoons}}$	$RH_5{}^+$	K_5
$RH_5{}^+ + H_2\,(z)$	$\underset{k_{-6}}{\overset{k_6}{\rightleftharpoons}}$	$RH_6\,(z) + H^+$	K_6
$RH_6\,(z)$	$\underset{k_{-7}}{\overset{k_7}{\rightleftharpoons}}$	$RH_6\,(g)$	K_7
$R\,(g) + 3H_2$	$\underset{H^+}{\overset{k^R_{H_2}}{\longrightarrow}}$	$RH_6\,(g)$	$k^R_{H_2}$

$$r = k_4\,[RH^+]\,[H_2(z)]$$

$$\frac{r}{[H^+]} = \underbrace{k_4 K_3 K_2 K_1}_{k^R_{H_2}}\, p_R p_{H_2}$$

Scheme 3. Elementary steps proposed for hydrogenation of benzene and toluene over HBEA. The step highlighted in bold is considered as rate-determining. The notations *g* and *z* in the parenthesis denote gas phase and intrazeolite phase, respectively.

pressures of species *i* and *j* along the catalyst bed, $\dot{V}$ represents total volumetric flow rate of inlet feed measured at ambient conditions, p_o represents inlet partial pressure of the reactant, and w_o represents total number of H^+ in the catalyst bed. The boundary condition for this model can be stated as $p_i/p_o = 1$ for reactants and 0 for products at inlet ($y = 0$).

To simplify the model, the two methylcyclopentene isomers shown in Scheme 5 were lumped as one species, and rates of interconversion between cyclohexene and methycyclopentenes were considered to depend linearly on cyclic olefin pressure while rates of their hydrogenation were considered to depend linearly on cyclic olefin and H_2 pressures. Under these assumptions, the differential material balance equations for (1) cyclohexene, (2) methylcyclopentenes, and (3) methylcyclopentane can be written as Eqs. (5)–(7), respectively.

$$\left(\frac{\dot{V}}{RT}\right)\frac{d(p_1/p_o)}{dy} = [k^{C5}_{2b}\,(p_2/p_o) - k^{C6}_{2f}\,(p_1/p_o) - k^{C6}_{3}\,(p_1/p_o)\,p_{H_2}] \times w_o \quad (5)$$

$$\left(\frac{\dot{V}}{RT}\right)\frac{d(p_2/p_o)}{dy} = [k^{C6}_{2f}\,(p_1/p_o) - k^{C5}_{2b}\,(p_2/p_o) - k^{C5}_{3}\,(p_2/p_o)\,p_{H_2}] \times w_o \quad (6)$$

$$\left(\frac{\dot{V}}{RT}\right)\frac{d(p_3/p_o)}{dy} = [k^{C6}_{3}(p_1/p_o)p_{H_2} + k^{C5}_{3}(p_2/p_o)p_{H_2}] \times w_o. \quad (7)$$

We used 'ode45' function in MATLAB to solve this set of coupled differential equations in order to obtain partial pressure profiles of all species along the catalyst bed (y = 0:1) and simultaneously used 'lsqcurvefit' to ascertain best estimates of the four unknown kinetic parameters ($k^{C6}_{2f}, k^{C5}_{2b}, k^{C6}_{3}$, and k^{C5}_{3}) with the objective of minimizing the difference between values of p_i/p_o at $y = 1$ obtained from MATLAB simulations and those measured during experiments; the code used is included in Section S7 of SI. In total, 44 different data sets including variations in inlet partial pressures of cyclohexene/1-methyl-1-cyclopentene (0.09–0.21 × 10^{-5} bar) and H_2 (0.075–0.375 bar) while keeping total pressure fixed at 1.52 bar (balanced by a combination of toluene, argon, and helium), and variations in inlet space velocities of cyclohexene/1-methyl-1-cyclopentene (0.09–0.53 $mol_{C_6H10}\ (mol_{H^+}{\cdot}ks)^{-1}$) were fitted together to estimate the unknown kinetic parameters. The values

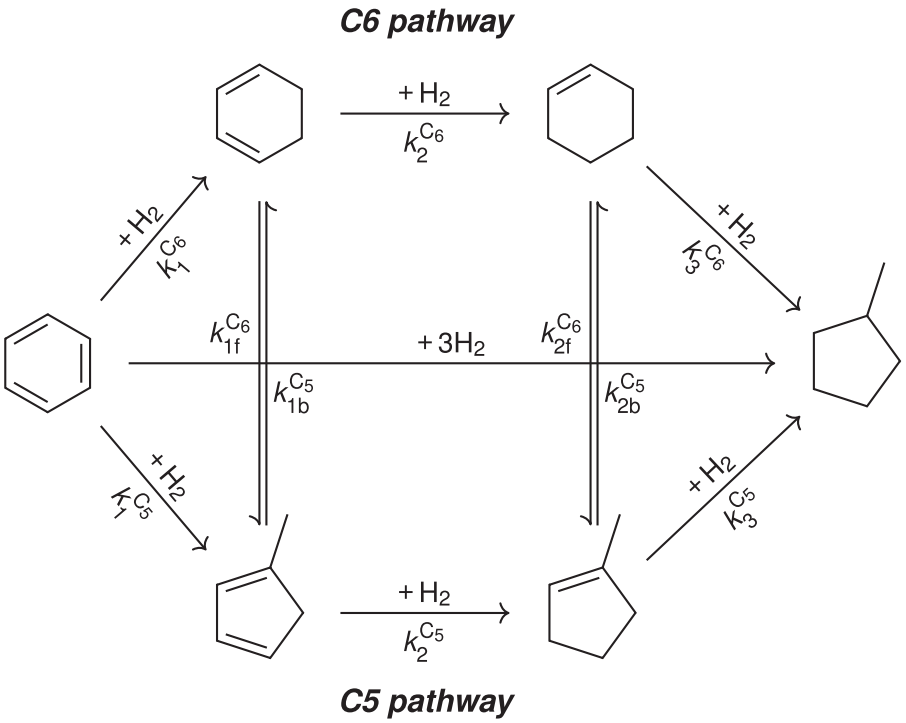

Scheme 4. Schematic showing sequential hydrogenation steps during co-reaction of benzene and H_2 over HBEA leading to methylcyclopentane synthesis. The top sequence involving intermediate formation of cyclohexadiene and cyclohexene is referred as the 'C6 pathway' while the bottom sequence involving intermediate formation of methylcyclopentadiene and methylcyclopentene is referred as the 'C5 pathway'.

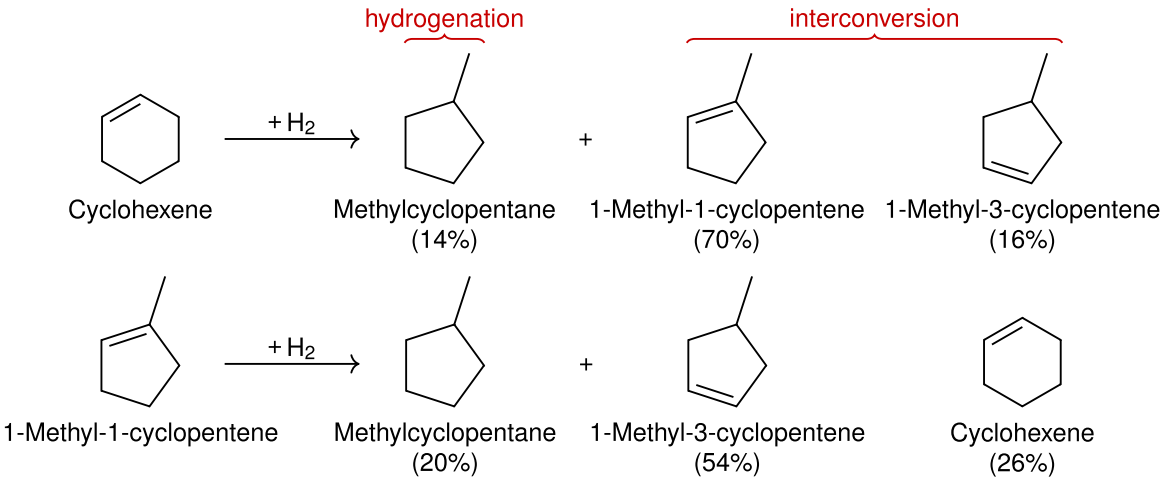

Scheme 5. Effluent product distribution observed during co-reaction of 0.11×10^{-5} bar cyclohexene and 1-methyl-1-cyclopentene with 0.15 bar H_2 over HBEA at 623 K and 0.15 mol_{C_6H10} $(mol_{H^+} \cdot ks)^{-1}$. The conversion levels in case of cyclohexene and 1-methyl-1-cyclopentene feed were 88% and 26%, respectively. The overall composition of the influent stream was 0.11×10^{-5} bar cyclohexene/1-methyl-1-cyclopentene, 59×10^{-5} bar toluene, 0.15 bar H_2, 1.35 bar He and 0.026 bar Ar, and total pressure was 1.52 bar.

thus obtained along with their 95% confidence intervals are listed in Table 1 ; Fig. 2 shows parity between simulated (p_{sim}) and experimentally measured (p_{exp}) exit partial pressures of all species.

From Table 1 and Fig. S5 of SI, we note the following two observations: (i) hydrogenation rate constants of cyclohexene and methylcyclopentenes (k_3^{C6} = 207.0 and k_3^{C5} = 45.17 mol (mol H^+)$^{-1}$ s^{-1} (bar C_6H_{10})$^{-1}$ (bar H_2)$^{-1}$, respectively at 623 K) are six orders of magnitude larger than the measured rate constant of benzene hydrogenation ($k_1^{C6/C5}$ = 0.00029 mol (mol H^+)$^{-1}$ s^{-1} (bar C_6H_6)$^{-1}$ (bar H_2)$^{-1}$ at 623 K) which corroborates our conclusion that intermediates generated after the rate-determining first hydrogenation step react rapidly to the final product during benzene hydrogenation; and (ii) although the rate constant of cyclohexene hydrogenation is larger (~4.6×) than the corresponding value for methylcyclopentenes hydrogenation, the rate constant of its conversion to methylcyclopentenes is also higher (~10×) than the corresponding value for methylcyclopentenes conversion to cyclohexene which implicates the likelihood of 'C6' and 'C5' pathways occurring concurrently during benzene hydrogenation to methylcyclopentane.

3.2. Hydrogenation of alkenyl-substituted benzenes and polycyclics on HBEA

Styrene and naphthalene were chosen as representative alkenyl-substituted benzenes and polycyclics in this study. Reactions of styrene (diluted with toluene) and naphthalene (diluted with benzene) with excess H_2 (H_2/R > 28,000) at 673 K on HBEA under differential conditions (<11%C conversion) resulted in the exclusive formation of ethylbenzene in case of styrene, and a combination of 1,4-dihydronaphthalene, tetralin, 1-methyl-1-propenyl-benzene, 1-ethenyl-4-ethyl-benzene, and 1-propenyl-benzene (likely resulting from protolytic cracking of 1-methyl-1-propenyl-benzene with the corresponding methyl group reacting with benzene and naphthalene in the feed to form toluene and methylnaphthalene, respectively, both of which were observed in the effluent) in case of naphthalene as shown in Scheme 6 along with the measured selectivities. Fig. 3 shows that turnover rates (per H^+) of both styrene and naphthalene hydrogenation vary linearly with partial pressure of the aromatic and H_2, as was the case during benzene and toluene hydrogenation (Fig. 1). This again stipulates that the observed kinetic behavior can be quantitatively described by the rate expression shown in Eq. (1) and rationalized by the sequence of elementary steps shown in Scheme 3 where the first hydrogenation step is rate-determining regardless of the number of moles of H_2 incorporated in the final products observed in the effluent. The effective second-order rate constants are enumerated as (38.2 ± 5.7) for styrene hydrogenation at 623 K and (0.71 ± 0.24) for naphthalene hydrogenation at 673 K with the corresponding units being mol (mol H^+)$^{-1}$ s^{-1} (bar R)$^{-1}$ (bar H_2)$^{-1}$. The temperature dependence of measured hydrogenation rate constants of both styrene and naphthalene is shown in Fig. S5 of SI, and apparent enthalpic and entropic barriers thus obtained are tabulated in Table S2 of SI. For comparison with other hydrogenation rate constants reported at 673 K, the corresponding value for styrene is 68.1 mol (mol H^+)$^{-1}$ s^{-1} (bar C_8H_8)$^{-1}$ (bar H_2)$^{-1}$ as obtained from Fig. S5 of SI.

Table 1
Estimates of kinetic parameters (along with their 95% confidence intervals) dictating interconversion between cyclohexene and methylcyclopentenes, and their hydrogenation to methylcyclopentane at 623 K over HBEA obtained using MATLAB simulations. Scheme 5 illustrates the specific reactions dictated by these parameters.

Kinetic parameter	Estimated value	Units
k_{2f}^{C6}	481.6 ± 11.2	mol (mol H^+)$^{-1}$ s^{-1} (bar R)$^{-1}$
k_{2b}^{C5}	48.02 ± 3.97	mol (mol H^+)$^{-1}$ s^{-1} (bar R)$^{-1}$
k_3^{C6}	207.0 ± 21.2	mol (mol H^+)$^{-1}$ s^{-1} (bar R)$^{-1}$ (bar H_2)$^{-1}$
k_3^{C5}	45.17 ± 7.08	mol (mol H^+)$^{-1}$ s^{-1} (bar R)$^{-1}$ (bar H_2)$^{-1}$

4. Discussion

We note that while benzene and toluene hydrogenation result primarily in formation of their triply-hydrogenated five-membered ring analogs, hydrogenation of styrene results only in ethylbenzene formation via hydrogenation of the ethenyl-substituent group while leaving the benzene ring intact (Schemes 2 and 6). Co-reacting ethylbenzene with excess H_2 (H_2/C_8H_{10} ~10^4) at 673 K in independent studies also did not yield any hydrogenated analogs of ethylbenzene and instead, ethylbenzene underwent cracking to form benzene and ethene. Similarly, co-reacting p-xylene with excess H_2 (H_2/C_8H_{10} ~10^7) at 673 K also did not result in formation of its hydrogenated analogs and instead, p-xylene underwent isomerization to m-xylene, and disproportiona-

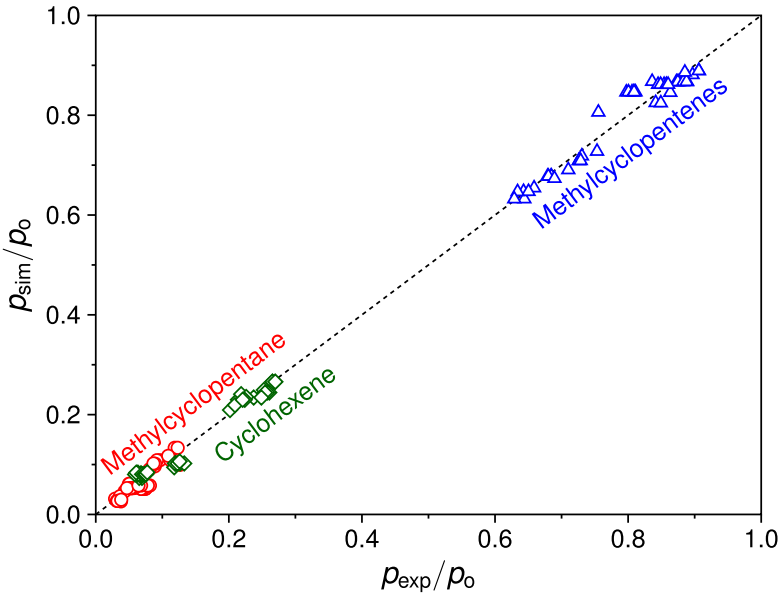

Fig. 2. Parity plot between simulated (p_{sim}) and experimentally (p_{exp}) measured exit partial pressures (normalized by inlet partial pressures of the reactant (p_o)) of cyclohexene (◇), methylcyclopentenes (△), and methylcyclopentane (○) during independent experiments involving co-reactions of cyclohexene or 1-methyl-1-cyclopentene (0.09–0.21 × 10^{-5} bar) with H_2 (0.075–0.375 bar) at 623 K and 0.09–0.53 mol_{C_6H10} $(mol_{H^+} \cdot ks)^{-1}$ over HBEA. The overall composition of the influent stream was 0.09–0.21 × 10^{-5} bar cyclohexene or 1-methyl-1-cyclopentene, 47.3–110.3 × 10^{-5} bar toluene, 0.075–0.375 bar H_2, 1.20–1.40 bar He and 0.026 bar Ar, and total pressure was 1.52 bar.

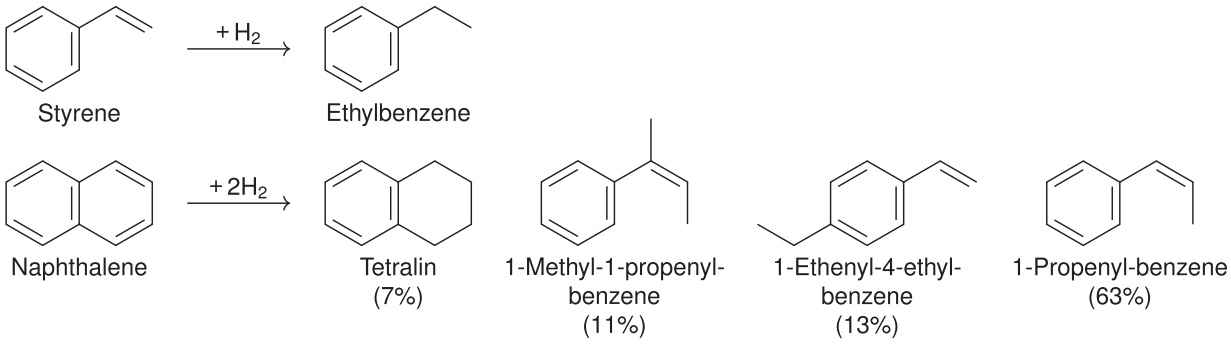

Scheme 6. Typical product distribution observed during styrene and naphthalene hydrogenation over HBEA at 673 K. For naphthalene hydrogenation, the balance 6% selectivity belongs to the singly-hydrogenated analog of naphthalene—1,4-dihydro-naphthalene—and the overall conversion level was ~4% during its feed at 8.7 × 10^{-5} bar with 3.02 bar H_2 and 4.7 $mol_{C_{10}H8}$ $(mol_{H^+} \cdot ks)^{-1}$; the overall composition of the influent stream was 8.7 × 10^{-5} bar naphthalene, 304.5 × 10^{-5} bar benzene, 3.02 bar H_2, and 0.068 bar Ar, and total pressure was 3.09 bar.

tion to toluene and trimethylbenzenes. These observations suggest that presence of an alkyl-substituent or more than one methyl-substituent on the benzene ring introduces secondary reaction pathways which prevent its activation by H_2 over zeolitic protons. The mechanistic origins of this observation are still not yet fully understood.

As deduced by differences in measured rate constants at 673 K, both styrene and naphthalene are observed to exhibit significantly higher (>20,300× and >210×, respectively) propensity for hydrogenation compared to benzene/toluene. The higher reactivity of styrene compared to benzene/toluene can be attributed to (i) retention of aromaticity in ethylbenzene observed during styrene hydrogenation compared to the triply-hydrogenated analogs observed during benzene/toluene hydrogenation, and (ii) the presence of π-electron delocalization in the benzyl carbenium ion ($C_6H_5 - CH^+ - CH_3$) that is likely formed upon interaction of the ethenyl-substitutent group in styrene with H^+ compared to arenium ions ($C_6H_7^+$ and $C_6H_6^+ - CH_3$) that are likely formed upon interaction of benzene and toluene with H^+ in step 3 of Scheme 3 [30]. The higher reactivity of naphthalene compared to benzene is consistent with similar reactivity trends observed over metal sulfide catalysts [31] and is likely related to lower resonance energy per ring in naphthalene (~117 kJ/mol) compared to benzene (~167 kJ/mol) even though the overall resonance stabilization is higher in naphthalene (~314 kJ/mol) [32,26].

In their study on aliphatics hydrogenation, Arora et al. [13] reported effective second-order hydrogenation rate constants of ethene, propene, and 1,3-butadiene over this HBEA sample as 0.020, 0.33, and 2.3 mol $(mol\ H^+)^{-1}\ s^{-1}$ $(bar\ R)^{-1}$ $(bar\ H_2)^{-1}$, respectively at 673 K. Comparing these values with those measured for benzene and toluene, we infer that both olefins and polyenes are more reactive (>6× larger rate constants) with H_2 than benzene/toluene. This behavior can likely be ascribed to resonance stabilization present in the latter. Further, akin to the observation of higher reactivity of alkenyl-substituted benzenes (styrene) compared to methyl-substituted benzenes (benzene and toluene), polyenes (1,3-butadiene) are observed to be more reactive (>7× larger rate constant) than olefins (ethene and pro-

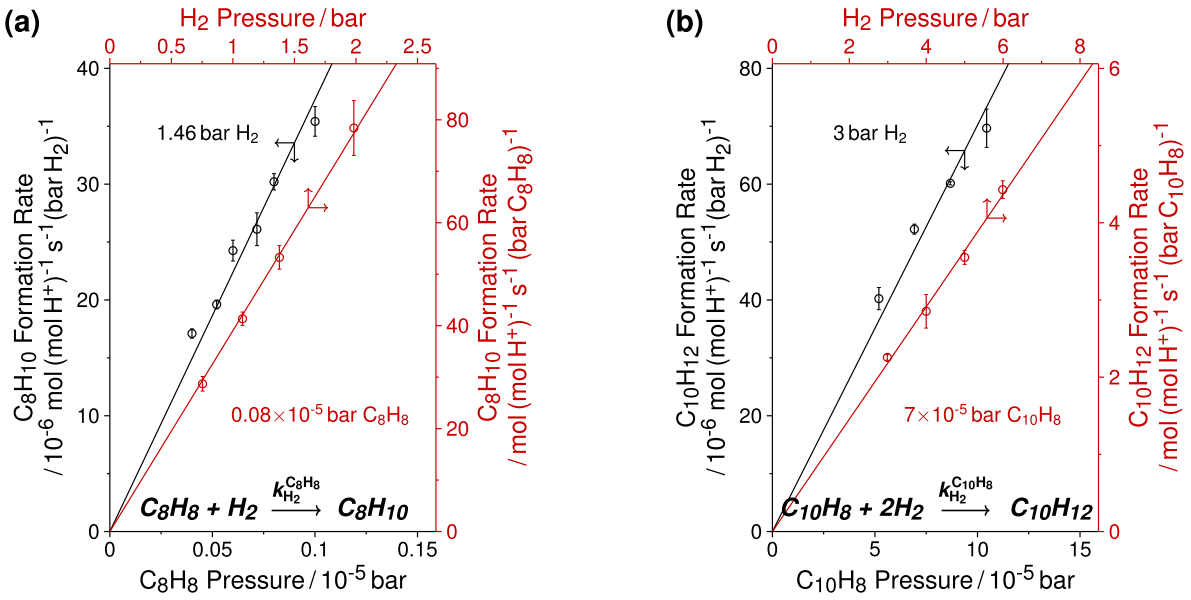

Fig. 3. Dependence of turnover rates (per H^+) of (a) styrene and (b) naphthalene hydrogenation on partial pressure of the aromatic (*bottom-left* axes) and H_2 (*top-right* axes) during reactions of (a) styrene with H_2 at 623 K and 0.4–1.0 mol_{C_8H8} $(mol_{H^+}{\cdot}ks)^{-1}$, and (b) naphthalene with H_2 at 673 K and 2.7–5.3 $mol_{C_{10}H8}$ $(mol_{H^+}{\cdot}ks)^{-1}$ over HBEA. The solid lines represent a linear fit to experimental data and quantities listed along these lines indicate partial pressure of the aromatic or H_2 held constant while varying the partial pressure of the other reagent. The vertical bars on each data point reflect standard-error associated with each measurement. For styrene hydrogenation, overall composition of the influent stream was 0.04–0.1 × 10^{-5} bar styrene, 14.8–37.0 × 10^{-5} bar toluene, 0.075–1.98 bar H_2 and 0.012 bar Ar, and total pressure was 1.38–2.00 bar. For naphthalene hydrogenation, overall composition of the influent stream was 5–10 × 10^{-5} bar naphthalene, 0.00175–0.0035 bar benzene, 3.0–6.0 bar H_2 and 0.068 bar Ar, and total pressure was 3.08–6.08 bar.

pene). Based on these observations, we conclude that both unsaturated intermediates (polyenes and alkenyl-substituted benzenes) and polycyclics formed in formaldehyde-mediated alkylation pathways during methanol conversion (Scheme 1) are more prone to reaction with H_2, which underlies the effectiveness of high-pressure H_2 cofeeds in prolonging catalyst lifetimes during MTH over Brønsted acid zeolites [12–15,13].

5. Conclusions

Hydrogenation of benzene, toluene, styrene, and naphthalene with excess H_2 on HBEA under differential conditions occurs with rates that vary linearly with aromatic and H_2 pressures implicating the first hydrogenation step to be rate-determining. Benzene and toluene hydrogenation results primarily in formation of five-membered cycloalkanes in contrast to metal-based catalysts which typically produce six-membered ring species. Independent studies involving reactions of cyclohexene and methylcyclopentenes with H_2 reveal that rate constants of their interconversion and hydrogenation to methylcyclopentane are significantly larger than the measured rate constant of benzene hydrogenation to methylcyclopentane, demonstrating plausibility of both methylcyclopentadiene/methylcyclopentene and cyclohexadiene/cyclohexene formation during benzene conversion. Hydrogenation of styrene occurs with the highest rate among the aromatics considered and exclusively produces ethylbenzene keeping the benzene ring intact. Co-reacting ethylbenzene or p-xylene with excess H_2 does not result in hydrogenation of the benzene ring, but instead these reactants undergo secondary reactions including cracking, isomerization, and disproportionation to form benzene and toluene which subsequently can be activated by H_2. Hydrogenation of naphthalene results primarily in ring open products at rates that are also higher than those measured for benzene/toluene and can likely be related to lower resonance energy per ring in naphthalene compared to benzene. These studies demonstrate feasibility of aromatics hydrogenation on zeolitic protons, and the higher reactivity of alkenyl-substituted benzenes and polycyclics compared to methyl-substituted benzenes provides a mechanistic basis for the reported enhancements in MTH lifetime with H_2 cofeeds.

Declaration of Competing Interest

The authors declare that they have no known competing financial interests or personal relationships that could have appeared to influence the work reported in this paper.

Acknowledgements

We acknowledge (i) Dow through the University Partnership Initiative and the National Science Foundation (CBET 1701534) for financial support, (ii) Dr. Andrzej Malek, Dr. Davy L. S. Nieskens, and Dr. Joseph DeWilde from Dow for helpful technical discussions, (iii) Dr. Nicholas Seaton from the University of Minnesota Characterization Facility, which receives partial support from the National Science Foundation through the Materials Research Science and Engineering Centers program, for providing the SEM-EDS measurements and SEM images of the HBEA sample, (iv) Mr. Xinyu Li from the University of Minnesota for providing the X-ray diffractogram and pyridine IR spectra of the HBEA sample, and (v) Ms. Zhichen Shi from the University of Minnesota for providing the NH_3 TPD data of the HBEA sample.

Appendix A. Supplementary material

Supplementary data associated with this article can be found, in the online version, at https://doi.org/10.1016/j.jcat.2019.12.039.

References

[1] T. Sano, H. Hagiwara, K. Okabe, H. Okado, K. Saito, H. Takaya, Sekiyu Gakkaishi 29 (1986) 89–92.
[2] T. Sano, H. Shoji, K. Okabe, K. Saito, H. Hagiwara, T. Hosoya, H. Takaya, Sekiyu Gakkaishi 29 (1986) 257–261.

[3] T. Sano, K. Okabe, H. Hagiwara, H. Takaya, H. Shoji, K. Matsuzaki, J. Mol. Catal. 40 (1987) 113–117.
[4] A.M. Gadalla, T. Chan, R.G. Anthony, Int. J. Chem. Kinet. 15 (1983) 759–774.
[5] J. Kanai, J.A. Martens, P.A. Jacobs, J. Catal. 133 (1992) 527–543.
[6] T. Sano, Sekiyu Gakkaishi 35 (1992) 119–127.
[7] J. Meusinger, J. Liers, A. Mosch, W. Rescheitilowski, J. Catal. 148 (1994) 30–35.
[8] J. Meusinger, A. Corma, J. Catal. 152 (1995) 189–197.
[9] R. Gounder, E. Iglesia, J. Catal. 277 (2011) 36–45.
[10] S. Senger, L. Radom, J. Am. Chem. Soc. 122 (2000) 2613–2620.
[11] B. Chan, L. Radom, J. Am. Chem. Soc. 130 (2008) 9790–9799.
[12] S.S. Arora, D.L.S. Nieskens, A. Malek, A. Bhan, Nat. Catal. 1 (2018) 666–672.
[13] S.S. Arora, Z. Shi, A. Bhan, ACS Catal. 9 (2019) 6407–6414.
[14] D.L.S. Nieskens, J.D. Lunn, A. Malek, ACS Catal. 9 (2019) 691–700.
[15] X. Zhao, J. Li, P. Tian, L. Wang, X. Li, S. Lin, X. Guo, Z. Liu, ACS Catal. 9 (2019) 3017–3025.
[16] S. Muller, Y. Liu, M. Vishnuvarthan, X. Sun, A.C. van Veen, G.L. Haller, M. Sanchez-Sanchez, J.A. Lercher, J. Catal. 325 (2015) 48–59.
[17] S. Muller, Y. Liu, F.M. Kirchberger, M. Tonigold, M. Sanchez-Sanchez, J.A. Lercher, J. Am. Chem. Soc. 138 (2016) 15994–16003.
[18] J.S. Martinez-Espin, K. De Wispelaere, T.V.W. Janssens, S. Svelle, K.P. Lillerud, P. Beato, V. Van Speybroeck, U. Olsbye, ACS Catal. 7 (2017) 5773–5780.
[19] A. Hwang, M. Kumar, J.D. Rimer, A. Bhan, J. Catal. 346 (2017) 154–160.
[20] S.S. Arora, A. Bhan, J. Catal. 356 (2017) 300–306.
[21] Y. Liu, F.M. Kirchberger, S. Miiller, M. Eder, M. Tonigold, M. Sanchez-Sanchez, J. A. Lercher, Nat. Commun. 10 (2019) 1462.
[22] A. Hwang, A. Bhan, Acc. Chem. Res. 52 (2019) 2647–2656.
[23] J.C. Jansen, E.J. Creyghton, S.L. Njo, H. Van Koningsveld, H. Van Bekkum, Catal. Today 38 (1997) 205–212.
[24] P. Weisz, C. Prater, Adv. Catal. 6 (1954) 143–196.
[25] K.J. Yoon, M.A. Vannice, J. Catal. 82 (1983) 457–468.
[26] A. Stanislaus, B.H. Cooper, Catal. Rev.-Sci. Eng. 36 (1994) 75–123.
[27] J. Wang, H. Chen, Q. Li, React. Kinet. Catal. Lett. 69 (2000) 277–284.
[28] J.F. Haw, Phys. Chem. Chem. Phys. 4 (2002) 5431–5441.
[29] A. Primo, H. Garcia, Chem. Soc. Rev. 43 (2014) 7548–7561.
[30] R. Hoffman, J. Chem. Phys. 40 (1964) 2480–2488.
[31] A.V. Sapre, B.C. Gates, Ind. Eng. Chem. Process Des. Dev. 20 (1981) 68–73.
[32] C.P. Moreau, P. Geneste, Theor. Asp. Heterog. Catal., Springer, Netherlands: Dordrecht, 1990, pp. 256–310.